12-2018

Ca2+ - Induced Structural Change of Multi-Domain Collagen Binding Segments of Collagenases ColG and ColH from Hathewaya histolytica

Christopher Eric Ruth
University of Arkansas, Fayetteville

Ca^{2+} - Induced Structural Change of Multi-Domain Collagen Binding Segments of Collagenases ColG and ColH from *Hathewaya histolytica*

A thesis submitted in partial fulfillment
of the requirements for the degree of
Master of Science in Chemistry

by

Christopher E. Ruth
Bethune Cookman University
Bachelor of Science in Chemistry, 2015

December 2018
University of Arkansas

This thesis is approved for recommendation to the Graduate Council.

_____
Joshua Sakon, Ph.D.
Thesis Director

_____
Frank Millett, Ph.D.
Committee Member

_____
Roger Koeppe Ph.D.
Committee Member

_____
Suresh Thallapuranam, Ph.D.
Committee Member

_____
Matt McIntosh, Ph.D.
Committee Member

ABSTRACT

Hathewaya histolytica, previously renamed as *Clostridium histolyticum,* secretes at least two collagenases, ColH and ColG, that allow for degradation of extracellular matrices of animal tissue. *Hathewaya histolytica* virulence factors are proposed to undergo domain rearrangement upon secretion from the bacteria to the host. In order to accomplish this, collagenases seek the least ordered regions in collagen to efficiently disassemble the fibril. Two types of domains, Polycystic Kidney Disease-like (PKD) and Collagen Binding Domain (CBD), direct the collagenases ability to disassemble the fibril. Calcium dependent structural change have been reported to increase in thermal stability and in tighter collagen binding for CBD. Different surface properties and indications of varied dynamics suggest unique roles for the PKD-like domains in ColG and in ColH. These domains are useful in anchoring fused growth factors to lesions. Most recent results show that use of multi-domain targeting segments result in more efficacious preclinical outcomes in various animal models. Single domain targeting segments have been biophysically characterized; however, multi-domain targeting segments have not been biophysically characterized. In this study, Small Angle X-Ray Scattering (SAXS) methods were used to monitor calcium dependent structural change of multi-domain segments, i.e. PKD1-PKD2-CBD and PKD-CBD1-CBD2 (Ruth and Sakon 2017). All SAXS data were collected at 10°C through the Advanced Light Source at Berkley National Lab (Otwinowski and Minor 1997) (Classen, Hura et al. 2013). The average of 33 beam exposures were collected and processed through primusqt (Konarev, Petoukhov et al. 2006). Genes for type II secretion system are recently reported in the genus. The bacteria apparently evolved to take advantage of calcium concentration differential from inside the bacteria and the extracellular matrix to efficiently secrete virulence factors

ACKNOWLEDGEMENTS

I would like to take this time to acknowledge the supported grant from NIGMS (P20 GM103429) at NIH INBRE, ABI, and the University of Arkansas Graduate School. To the department of Chemistry and Biochemistry, for continuing to challenge me in every aspect for my future. Each of you have imparted lasting moments that will not easily be lost. To Latisha Puckett, PhD and Chris Mazzanti, PhD, who have continued to show me the importance of teaching Chemistry and for great friendship. I would also like to acknowledge Ryan Bauer, PhD and Perry Caviness, who have given me the best crash courses to x-ray crystallography. To, my fellow graduate students of 2015, thank you for bearing this time in arms with me. I never felt alone with each of you by my side. To my committee, your compassion and guided instruction is beyond value in this world. I thank you for believing in me and often times seeing in me what I generally don't see in myself. You have given timely correction that was sometimes hard to digest but has allowed me to be the best version of me.

Lastly, I would like to acknowledge my mentor, Joshua Sakon, PhD. I have been such a fortunate soul to have your guidance in my life. You have been far more than just a mentor to me. I know I can be hard to deal with at times (multiple times for multiple things). Even through all that you showed that you care for my well-being and that of my family time and time again. You were stern and direct when you needed to be, as well as caring and compassionate at other times. As cliché as this may sound, you are that crystal that we come into the research lab to work so hard to obtain. Thank you for your patience, love, and support for me these past few years.

DEDICATION

I dedicate this work to my wonderful family! To my three children, that have stolen my heart; Maija, Gabriel, and Autumn. To my siblings; Renee, Cory, Clarence, Terrance, and Charis. To my father, Clarence Ruth, I wish you could see this. To my number one fan from day one, my mother, Carol Hosendove. I love you all and could not have done this without you. Lastly, to my God in heaven with whom I find everything I need.

TABLE OF CONTENTS

LIST OF TABLES & FIGURES

INTRODUCTION:

Prior studies suggest calcium ions play a critical role in the structure and function of *Hathewaya histolytica* collagenases (Nishi, Matsushita et al. 1998, Matsushita, Koide et al. 2001). *Clostridium histolyticum*, recently renamed as *Hathewaya histolyitica*, secretes two classes of collagenases (ColG and ColH). The bacterium was reclassified into the *Hathewaya* based on 16S ribosomal sequence, but it remains as one of the histotoxic clostridia to cause gas gangrene (Lawson and Rainey 2016). ColG contains one PKD (s2) and two CBD (s3a and s3b) binding segment, while ColH contains two PKD (s2a and s2b) and one CBD (s3) binding segment (Matsushita, Koide et al. 2001). Both ColH and ColG contain a catalytic module (s1) of the mammalian matrix metalloproteases (MMPs) family. The binding segments of the collagenases, CBD and PKD-like, are not necessary to degrade gelatin (a non-triple helical, denatured form of collagen) or acid-solubilized collagen. However, they are necessary in order to degrade insoluble collagen fibrils.

Structures for each ColH and ColG segment have been determined individually. At this point, crystallographic methods have determined the holo peptidase segment (s1) (Eckhard, Schonauer et al. 2013), and apo (Eckhard, Schonauer et al. 2011) (Bauer, Janowska et al. 2015) for ColG and ColH. The holo (Eckhard and Brandstetter 2011, Eckhard, Schonauer et al. 2011, Eckhard, Schonauer et al. 2013) and apo (Eckhard, Schonauer et al. 2011) (Bauer, Janowska et al. 2015) s2 segment of ColG, apo (Bauer, Janowska et al. 2015) form of ColH s2a, holo form (Bauer, Wilson et al. 2013) of ColH s2b, apo and holo s3b of ColG (Wilson, J. et al. 2003) (Bauer, Wilson et al. 2013), holo s3 of ColH (Bauer, Wilson et al. 2013), as well as tandem CBD (s3as3b) of ColG in holo form(Caviness, Bauer et al. 2018) have all been determined structurally. Further structural studies are being conducted with the complete collagenase

molecule as multi-domain systems for ColH and ColG. The only multi-domain targeting segment that has been characterized biophysically is tandem CBD (s3a-s3b) of ColG, that has exhibited the tightest binding to a collagen (Matsushita, Koide et al. 2001). Recent biophysical studies for tandem CBD proposed the unique trans- collagen binding mechanism and Ca^{2+} dependent structural transformation (Caviness, Bauer et al. 2018).

Calcium ion induced activation has been known to increase thermal stability and catalytic activity of the enzymes. Simulation studies show that the presence of calcium significantly decreases the free energy barrier (Spiriti and Vaart 2010). When calcium ions are removed, it has been found that the trans state of the peptide bond was more thermodynamically stable over the cis state, which happens to align with prior crystallographic finding (Spiriti and Vaart 2010). Calcium also influences inter-segmental flexibility of full-length ColH (Ohbayashi, Matsumoto et al. 2013). Full-length ColG is proposed to undergo segment rearrangement induced by the presence of Ca^{2+} (Caviness, Bauer et al. 2018). It was additionally proposed that the chelation of calcium triggers the uncoiling of the linker to transition from α-helix (apo form) to β-sheet (holo form) (Wilson, J. et al. 2003) and reduces inter-segment flexibility (Sides 2012). This β-sheet formation causes the protein to become rigid and to increase the affinity for collagen (Philominathan, L. et al. 2009); (Wilson, J. et al. 2003). The calcium chelation site was also found in PKD-like domains (Bauer, Janowska et al. 2015); (Eckhard and Brandstetter 2011).

The K_d for Ca^{2+} of the CBD and PKD-like segments are equal to intracellular Ca^{2+} concentration of *H. histolytica* which is expected to be similar to *E. coli* at about 0.2-0.3 x 10^{-6} M (Holland, Jones et al. 1999). The mammalian tissue fluids with Ca^{2+} concentrations at 0.1 – 1.2M (Maurer and Hohenester 1997) (Nicholson 1980) (Brown, Vassilev et al. 1995) have been shown to be sufficient to trigger domain rearrangement. At lower calcium concentrations, collagenases

are anticipated to exhibit an elongated, and more flexible structure. This transformation of the enzyme could allow for more efficient secretion from the bacterial cell (Wilson, J. et al. 2003); (Bauer, Janowska et al. 2015); (Ohbayashi, Yamagata et al. 2012). It is to be noted that, *H. histolytica* transcribes collagenases and other toxins at record speed and rapid secretion to the extra-cellular matrix (ECM) results in significant tissue destruction. Conversely, at higher calcium concentrations, collagenases take on a more compact and protease resistant structure. It isn't known how Gram-positive pathogens secrete various toxins and virulence factors, across the bacterial cell wall and into the host tissues. (Melville 2015) Many recent studies, suggest the Type II Secretion System (TTSS/T2SS), or its homolog, play a major role in the secretion mechanism. It is the only system that is known to secrete protein substrates in the native folded state. (Yan, Yin et al. 2017) This TTSS, until recently, has been solely identified with Gram-negative bacterial pathogens. The more in-depth our understanding of the binding and secretion mechanism the more concrete our theory will become as we marry these two native processes.

Currently, ColG and ColH CBDs are being tested as a novel drug delivery system in combination with various growth factors. These growth factors, such as basic fibroblast growth factor (bFGF) have been previously studied with oriented collagen tubes (OCT) and led to formation of regenerated myelinated fibers at 4 weeks compared to the OCT alone (Fujimaki, Uchida et al. 2017). These fusion proteins of signal molecules bound to binding segments resulted in reduced dosage, extending half-life of signal molecules, and localizing its effect. *H. histolytica* collagen targeting segment from ColH, PKD-CBD, was the first used along with a localized EGF and basic FGF (Nishi, Matsushita et al. 1998). PKD-like segments do not bind tightly to collagen fibers, although the presence of s2b has been shown to enhance the overall binding (Matsushita, Koide et al. 2001) (Matsushita, Jung et al. 1998). PKD-like segment from

another bacterial source have been shown to swell collagen fibrils, but not unwind the fibrils (Wang 2010). This 'swelling' could be of value in targeting damaged collagen regions for collagenolysis. The PKD-CBD fused to basic FGF promoted bone fracture repair in various mice models. (Uchida 2013, Uchida 2015, Uchida 2016)

The CBD from ColH (s3) has been shown to extend half-life of Parathyroid hormone derived peptide 1-33 (Ponnapakkam 2014). The absence of PKD-like segment allowed for systemic distribution of PTH-CBD and accumulated to end plates of spinal column and growth plates of bones and skin (Ponnapakkam 2014). The s3 binds preferentially to under-twisted regions of collagen (Philominathan 2012), which may be abundant in rapidly remodeling ECM.

The tandem CBD (s3as3b) have shown to be more efficient in binding to insoluble collagen than does CBD (s3b) alone (Matsushita, Koide et al. 2001). The unique segment arrangement and Ca^{2+} interaction was recently described (Caviness, Bauer et al. 2018). The tandem CBD segment linked to basic FGF was more efficacious in repairing bone fracture than bFGF-CBD or bFGF-PKD-CBD (Sekiguchi 2018). The activation mechanism as well as suggestions for segment binding are described within this context.

Chapter 1 METHODS

Sample preparation to achieve optimum calcium conditions:

Targeting segments ColG and ColH were prepared by Professor Osamu Matsushita of Okayama University (Matsushita, Jung et al. 1998). Maxchelator software (http://maxchelator.stanford.edu/CaEGTA-TS.htm) was used to calculate pCa (pCa = -log[Ca^{2+}]) [Table 1]. Small Angle X-ray Scattering (SAXS) data was collected at these pCa conditions, constant at 10 °C, pH = 7.5. To produce the given pCa buffers, three stock solutions containing varied volumes of HEPES buffered saline (HBS), NaCl, EGTA (pH7.5) and $CaCl_2$ to a final volume of 50mL each, were prepared [Table 2]. The prepared stock solutions were then mixed together to produce the appropriate pCa buffers [Table 3]. Based on the need of volume from table 3, the total volume of table 2 was calculated to accommodate. It is to be mentioned, 8% glycerol was added to each pCa by going from 3% to 10% in increments of 1%.

Once the pCa conditions were created, 1mL of buffer and 2µL of protein sample was placed in Amicon Ultra-2 centrifugal filter devices. Additional buffer was then added to bring the final volume to 2mL. These devices were then spun down at 3500 x g(RCF) in swinging bucket rotors (4250) for 45 minutes. Once these samples were spun down they were loaded in an SDS and Native PAGE gel to determine the stability of the proteins. The Native PAGE, which was prepared with 20µL of 3x Native loading dye to 10µL of protein, showed almost no presence of bands after completion of electrophoresis. A silver stain was then utilized to reveal highly concentrated proteins [Figure 2], SDS was then run for more information. The SDS PAGE gel samples were prepared by adding 13µL DDH_2O and 2µL of the protein plus 10µL Laemmli loading dye. Once these sample were prepared in individual centrifuge tubes samples were centrifuged for 2 minutes, placed on heat block for 4 minutes, and then centrifuged once

again for 2 minutes. Samples were then carefully added to the wells and run at 40mA, 100V holding the amps constant. Single bands observed in the gel were faint but showed the expected molecular weights [Figure 1].

Sample preparation to prevent aggregation:

ColG sample were added in a volume of 20µL and 15mL pCa buffer. This was completed every 8-10 hours for a minimum of 3 cycles for dialysis. Once cycles completed samples were added to Amicon tubes at a ratio of 1mL pCa buffer, 3µL sample, and topped off with buffer up to 2mL. The samples were centrifuged down for 45 mins at 4250 rpm for 5 cycles to further concentrate the protein samples. To check for protein aggregation gel electrophoresis through native PAGE was conducted, no bands showed up using Coomassie Brilliant Blue thus a silver stain was used to visualize the bands on the gel. At high pCa, glycerol was initially added to potentially increase mono-dispersity of the sample. Glycerol was also added to the low pCa samples although it was found to not be as necessary to keep the protein monodispersed. This ensured a consistent set of buffer conditions for each calcium concentration [Ca^{2+}]. In continuing to ensure stability of the protein during shipment to Berkeley, influence of additives were examined for various ranges of polyethylene glycol (PEG) sizes. Of the concentrations tested (5-20%), 5% seemed to be the only concentration to maintain suitable conditions. Sucrose (%) was proven suitable as well. Glycerol in percentages of 4% or 6% were determined to be best suited for the pCa samples.

Bicinchoninic Acid (BCA) assay was then conducted to determine the protein concentration. The gradient range was from 2mg/mL to 0.25µg/µL. The samples were further concentrated in 5 cycles of 10mL. Fresh solutions were prepared of HBS-EGTA, HBS-Calcium,

and HBS in preparation of transport. Final well dilution calculations for the pCa samples were completed and samples were plated on a 96 well tray. The tray of prepared samples was then sent to SIBYLS beamline through the Advanced Light Source at Berkley National Lab. (Otwinowski and Minor 1997)

Small Angle X-ray Scattering (SAXS):

SAXS continues to emerge as an important technique for studying large-scale dynamic processes, ranging from protein folding to virus particle polymorphism (Tsuruta and Johnson 2006). SAXS measurements were completed for three concentration series per sample. Buffer from the last buffer exchange step during buffer equilibration was used to obtain background scattering for buffer subtraction. For the pCa series, the concentration of the ColG binding domains used range between 1, 3, and 5 mg/mL (Table 8). For ColH binding domains, 1-5 mg/mL concentrations were used (Table 7). All SAXS data were collected at 10°C at the Advanced Light Source at Berkley National Lab (Otwinowski and Minor 1997) using a Pilatus 2M detector (Classen, Hura et al. 2013, Dyer, Hammel et al. 2014). Sample to detector distance was 1.5 m, and X-ray wavelength was 1.127 Å. All data processing was accomplished using primusqt from the ATSAS 2.6.1 (pCa analysis) software package. Data from the concentration gradient that is not affected by either aggregation or detector saturation were extrapolated to infinite dilution. Determination of the radius of gyration (R_g), maximum diameter (D_{max}) as well as *ab initio* shape reconstruction of the extrapolated data for each model was carried out using the dammif function in primusqt. The χ values calculated at the end of each run indicated the agreement between the calculated scattering curve and the experimental scattering curve. The R_g, D_{max}, and χ values for ColG and ColH models are summarized in Tables 9 and 10, respectively.

The models shown in Figures 3-8 are the average of 10 models calculated from DAMAVER/DAMFILT and refined with DAMMIN. Primusqt was used for visualization and initial analysis of scattering data. Modeling program MiFIT (17) was used to position crystal structures of 5IKU for CBD and 4TN9 for PKD.

Table 1: Maxchelator Calculated Values

pCa 3 Conditions: EGTA: 0.0002M (0.2mM), Free Ca: 0.001M (1mM), pH: 7.5, Co: 10, N (Ionic): 0.1
Calculation Results
Name: Ca, Total: 0.00119998M, Free: 0.001M, Bound: 0.00019998M
Name: EGTA, Total: 0.0002M, Free: 1.143e-8M, Bound: 0.00019998M

pCa 4 Conditions: EGTA: 0.0002M (0.2mM), Free Ca: 0.0001M (0.1mM), pH: 7.5, Co: 10, N (Ionic): 0.1
Calculation Results
Name: Ca, Total: 0.00029988M, Free: 0.0001M, Bound: 0.00019988M
Name: EGTA, Total: 0.0002M, Free: 1.143e-7M, Bound: 0.00019988M

pCa 5 Conditions: EGTA: 0.0002M (0.2mM), Free Ca: 0.00001M (0.01mM), pH: 7.5, Co: 10, N (Ionic): 0.1
Calculation Results:
Name: Ca, Total: 0.00020886M, Free: 0.00001M, Bound: 0.0001988M
Name: EGTA, Total: 0.0002M, Free: 0.00000113M, Bound: 0.0001988M

pCa 6 Conditions: EGTA: 0.0002M (0.2mM), Free Ca: 0.000001M (0.001mM), pH: 7.5, Co: 10, N (Ionic): 0.1
Calculation Results:
Name: Ca, Total: 0.00019018M, Free: 0.000001M, Bound: 0.00018918M
Name: EGTA, Total: 0.0002M, Free: 0.00001081M, Bound: 0.00018918M

pCa 7 Conditions: EGTA: 0.0002M (0.2mM), Free Ca: 0.0000001M (0.0001mM), pH: 7.5, Co: 10, N (Ionic): 0.1
Calculation Results-
Name: Ca, Total: 0.00012733M, Free: 0.0000001M, Bound: 0.00012723M
Name: EGTA, Total: 0.0002M, Free: 0.00007276M, Bound: 0.00012723M

Table 2: Stock Buffer Concentrations

	HEPES	NaCl	EGTA	CaCl2
1)HBS-EGTA	10mM	100mM	0.4mM	0
2)HBS-Ca	10mM	100mM	0	2.4mM
3)HBS	10mM	100mM	0	0

Table 3: Total pCa Buffer Volumes

pCa	HBS-EGTA	HBS-Ca	HBS
3	50	50	0
4	50	12.49	37.51
5	50	8.68	41.32
6	50	7.73	42.27
7	50	4.54	45.46
Total	250	83.44	166.56

Table 4: Dilutions and absorbance readings at 562nm

Tube #	Dilution	A562
1	1/20	0.33481
2	1/2	1.26680
3	3/4	1.38640
4	0	0.13598
5	1	0.91370
6	2	1.24490
7	3	1.49040
8	4	1.30600
9	5	1.38390

Table 5: Concentration determinations for ColG pCa conditions (UV-Vis)

Sample	A280	Concentration (mg/mL)
ColG pCa 3	1.7107	2.4323
ColG pCa 4	9.971	2.1640
ColG pCa 5	7.52489	10.08927
ColG pCa 6	-value	7.626
ColG pCa 7	-value	8.22996

Table 6: Concentration determinations for ColH pCa conditions (UV-Vis)

Sample	A280	Concentration (mg/mL)
ColH pCa 3	0.07888	5.4833
ColH pCa 4	14.70189	15.451
ColH pCa 5	4.0565	2.21168
ColH pCa 6	-value	8.17649
ColH pCa 7	31.951	11.354

Table 7: ColH final SAXS well volumes and concentrations

ColH	High (uL)	(mg/mL)	Medium (uL)	(mg/mL)	Low (uL)	(mg/mL)
pCa 7	11.01	5	6.60	3	2.20	1
pCa 6	15.29	5	9.17	3	3.06	1
pCa 5	22.61	2	16.95	1.5	11.30	1
pCa 4	8.09	5	4.85	3	1.62	1
pCa 3	13.68	3	9.12	2	4.56	1

Table 7 (Cont.'d): ColH final SAXS well volumes and concentrations

Table 8: ColG final SAXS well volumes and concentrations

ColG	High (uL)	(mg/mL)	Medium (uL)	(mg/mL)	Low (uL)	(mg/mL)
pCa 7	15.19	5	9.11	3	3.04	1
pCa 6	16.39	5	9.83	3	3.28	1
pCa 5	12.39	5	7.43	3	2.48	1
pCa 4	23.10	2	17.33	1.5	11.55	1
pCa 3	20.56	2	15.42	1.5	10.28	1

Chapter 2 RESULTS

Molecular shape transformation was visualized by small angle X-ray scattering (SAXS). Various plots from the SAXS data are generated to assess protein stability, aggregation, and shape [Figures 3-8]. SAXS technique is resolution-limited and can sample only relatively long paired sets. The *pair-distribution function* [Figures 5 and 8] describes paired sets of all the points within a non-interacting molecule or a multi-molecular complex. *Guinier* plots [Figures 3 and 6] indicated that molecules did not form aggregates. *Kratky* plots [Figure 4 and 7] can be shown to determine globularity and flexibility of the protein. The distribution should be smooth and continuous and the longest represents the maximum diameter (D_{max}). The technique is useful in detecting conformational changes of a macromolecule in solution. Based on the ColG pair-distance distribution function plots, it can be indicated from the profile that the protein exhibits an oblong shape [Figure 5]. Also, as the presence of calcium increases it induces a noticeable change in pair-distribution plots. Similar changes in pair distribution function can be seen for Col H [Figure 8]. The smallest D_{max} was found for pCa 3 and 4 in ColG and ColH, respectively [Table 9]. D_{max} for pCa 6 is likely overestimated. The radius of gyration (Rg) was calculated using two methods. Rg for ColH stayed relatively unchanged; however, Rg for ColG altered at different pCa [Table 9]. Both ColG and ColH targeting domains are folded at all pCa values according to Kratky plots [Figures 4 and 7]. The R_g, D_{max}, and χvalues for each model are summarized in Table. The SAXS derived envelope for both ColG and ColH targeting segments are shown in Discussion section.

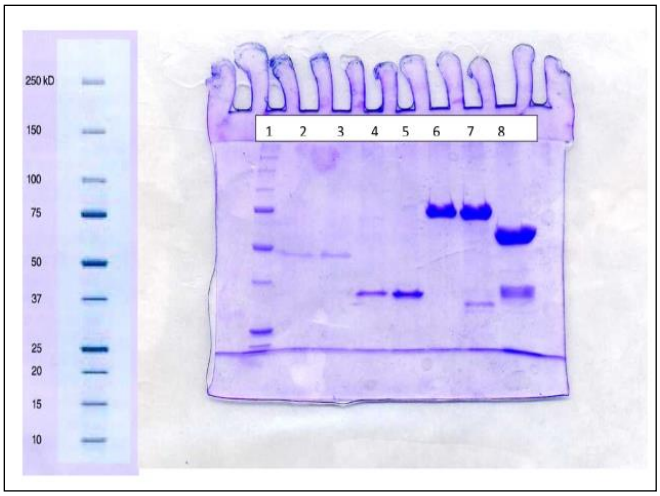

Figure 1: Initial SDS Gel to confirm protein stability. 12% SDS Gel.

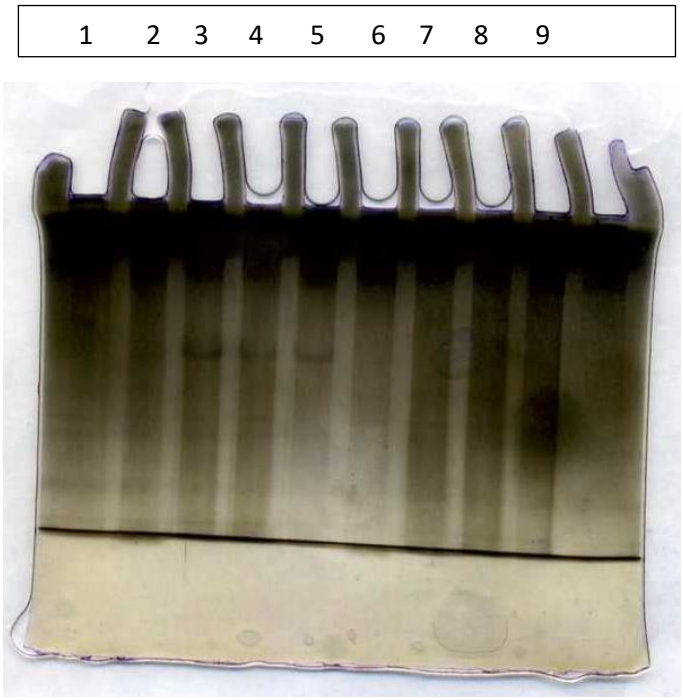

Figure 2: Native PAGE to assess protein stability. Lane 9 is overflow of the lane 8 protein (ColG s1).

I. Collagenase G Results

Table 9: Small Angle X-ray Scattering Statistics for ColG.

ColG	s2s3as3b	s2s3as3b	s2s3as3b	s2s3as3b
pCa	3.0	4.0	5.0	6.0
R_g (Å) Guinier Approx.	30±2.5	46±29.4	40±8.5	35±4.8
R_g (Å) Defined by Pd	32.06	34.95	53.28	38.58
D_{max} (Å)	126.72	115.56	196.85	152.35
χ	0.71	0.89	0.76	0.78
Q-range ($Å^{-1}$)	0.0226 0.1976	0.0304 0.3057	0.0226 0.1909	0.0203 0.1904

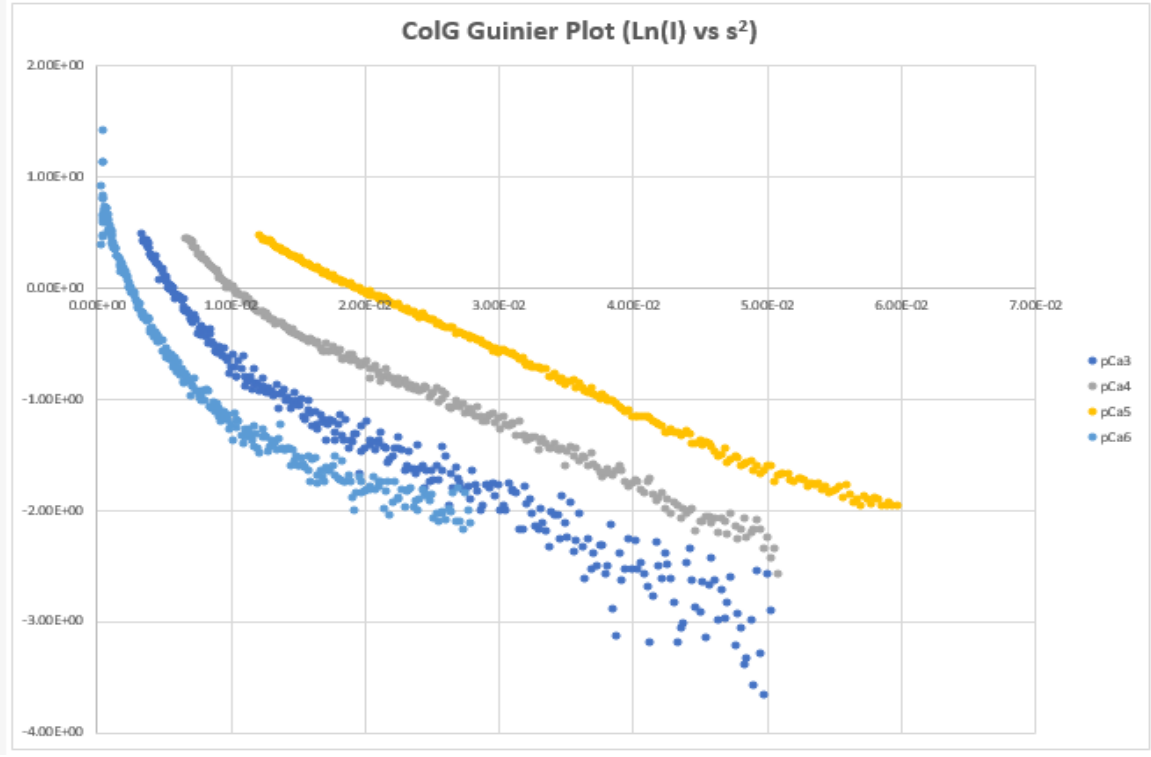

Figure 3: Collagenase G Guinier plot.

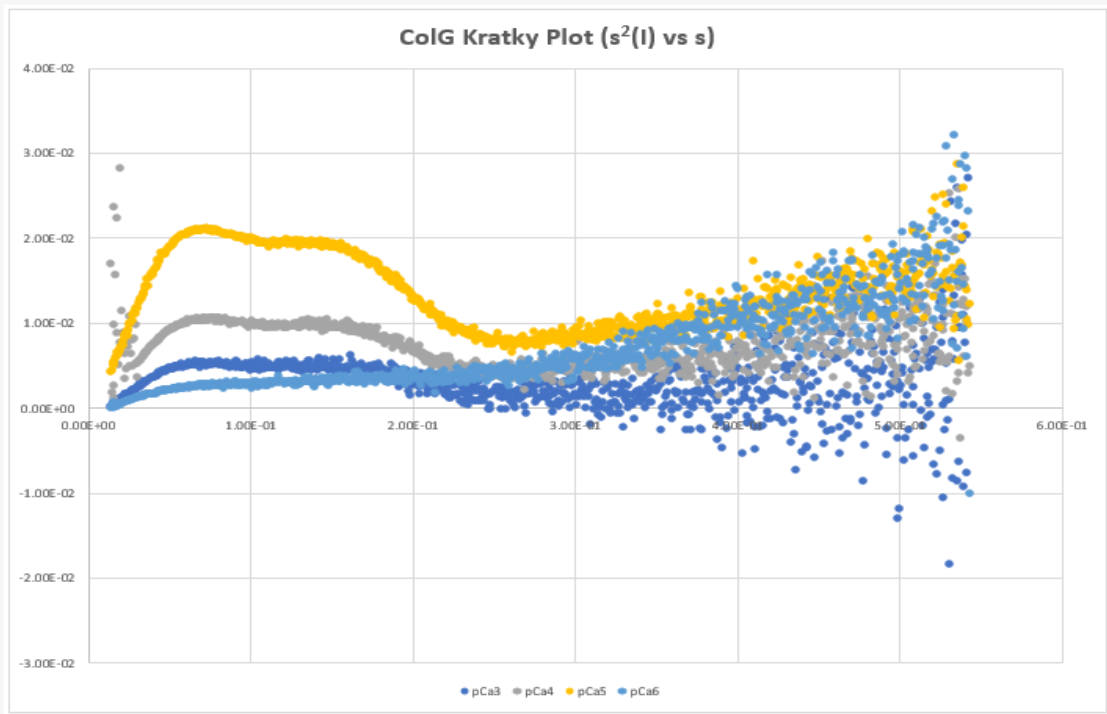

Figure 4: Collagenase G Kratky Comparison

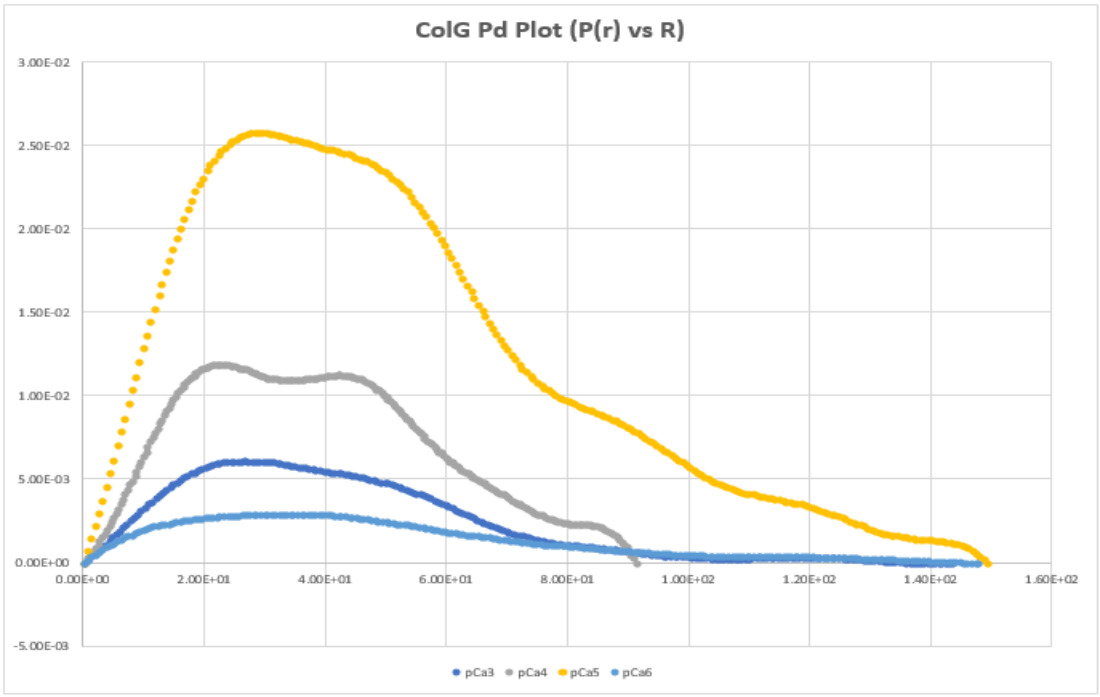

Figure 5: Collagenase G Pair-Distance Distribution Function Comparison

Fig. 3-5 (3) Guinier profile for s2-s3a-s3b at pCa 3-6. (4) Kratky profile for s2-s3a-s3b at pCa 3-7. (5) Pair-distance distribution function profile for s2-s3a-s3b at pCa 3-6.

II. Collagenase H Results

Table 10: Small Angle X-ray Scattering Statistics for ColH.

ColH	s2as2bs3	s2as2bs3	s2as2bs3	s2as2bs3	s2as2bs3
pCa	3.0	4.0	5.0	6.0	7.0
R_g (Å) Guinier Approx.	33±1.5	33±8.3	33±1.1	33±4.2	31±5.8
R_g (Å) Defined by Pd	35.57	35.74	35.94	36.92	33.33
D_{max} (Å)	135.68	130.94	142.08	152.37	147.18
χ	1.01	1.09	2.24	0.62	0.72
Q-range ($Å^{-1}$)	0.0181 0.2093	0.0242 0.1798	0.0242 0.2009	0.0192 0.1993	0.0282 0.2021

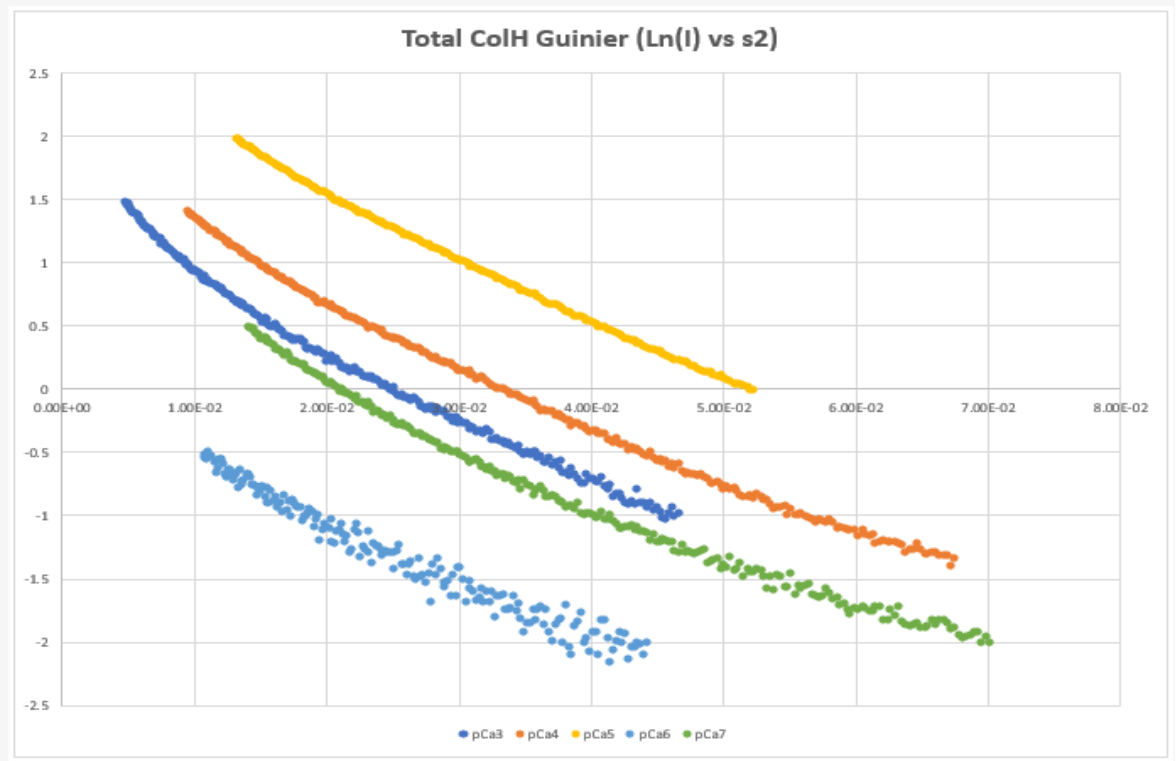

Figure 6: Collagenase H Guinier Comparison

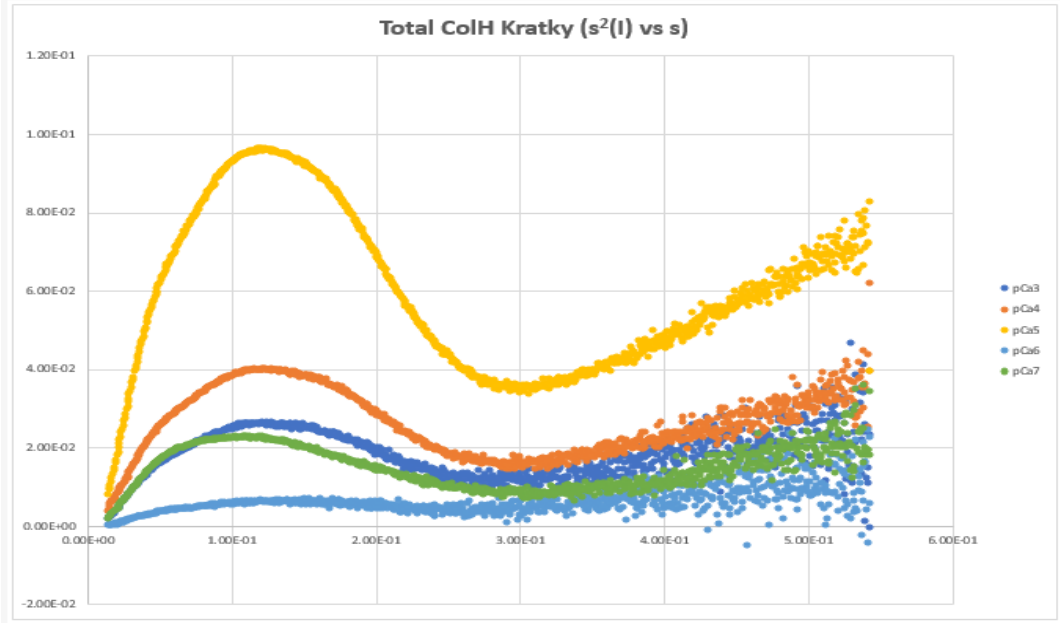

Figure 7: Collagenase H Kratky Comparison

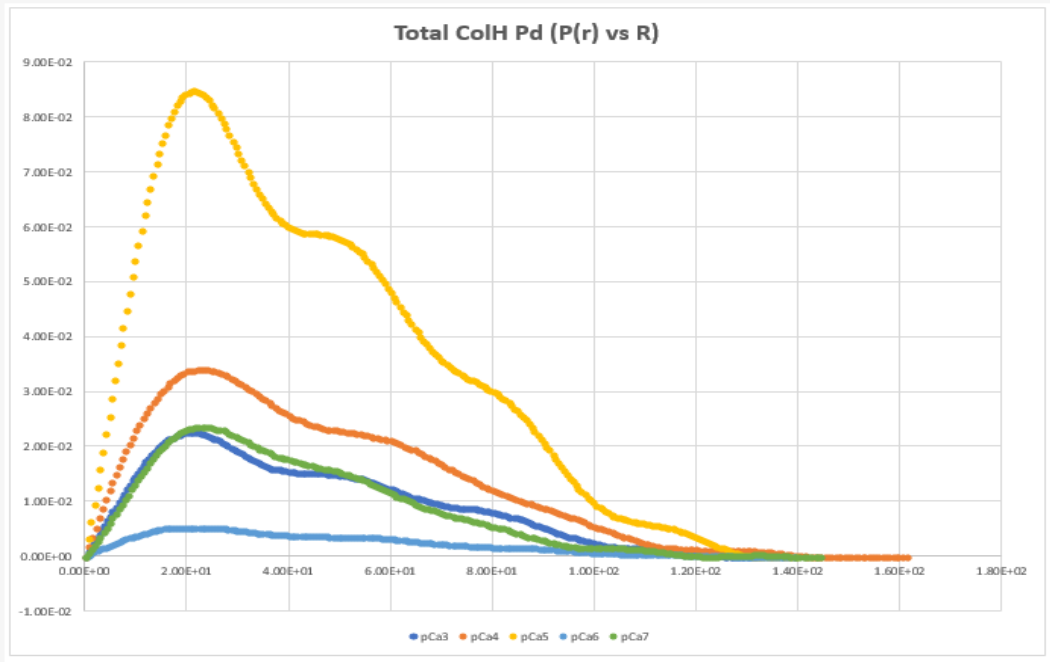

Figure 8: Collagenase H Pair-Distance Distribution Function

Fig. 6-8 (6) Guinier profile for s2a-s2b-s3 at pCa 3-7. (7) Kratky profile for s2a-s2b-s3 at pCa 3-7. (8) Pair-distance distribution function profile for s2a-s2b-s3 at pCa 3-7.

Chapter 3: DISCUSSION

The presence of calcium is proposed to initiate segment rearrangement in full-length ColH (Ohbayashi, Matsumoto et al. 2013). Calcium-induced structural transformation is also suspected in full-length ColG. Size exclusion chromatography for tandem CBD of ColG previously monitored the Ca^{2+}-induced reduction of the apparent molecular mass (Bauer, Janowska et al. 2017) (Caviness, Bauer et al. 2018). Additionally, the molecular shape transformation was visualized by small angle X-ray scattering (SAXS) for tandem CBD (Caviness, Bauer et al. 2018). These prior findings, along with the current discoveries, continue to build a more complete picture of the enzyme structure generating more support for the proposed mechanism.

The relevance of the role that calcium plays can possibly be discerned by looking at the difference in Ca^{2+} concentrations inside *H. histoyitica*, which is likely similar to the concentration inside *Escherichia coli* (0.2–0.3 μM; pCa 6.5-6.7) (Holland, Jones et al. 1999), and that of the host ECM (~1.2 mM; pCa~2.9), which may be exploited by the bacteria to facilitate rapid secretion into the host and enable enzyme activation (Caviness, Bauer et al. 2018). It is known that collagenases are secreted from bacteria into the host cell at record speeds (Addi 2016). SAXS results present an apparent structural change as that calcium environment becomes more concentrated that allows the assumption that the collagenase exhibits a more flexible orientation when inside of the bacteria. The use of the type 2 secretion system of bacteria in comparison to other well-known gram-positive secretion systems is steadily becoming an unabating likelihood. Current ongoing studies characterize this Type II Secretion System (TTSS), that is heavily found amongst Gram-negative bacteria, as a possible secretion system for Gram-positive pathogens. (Melville 2015)

The main function of the TTSS is to transport folded proteins from the periplasm through the outer membrane into the host. A two-step proposed mechanism of release for the enzyme [Figure 10] gives a proper prospective on the mechanism. This knowledge allows one to speculate the possible timing of the enzyme orientation change as well as speed of delivery to the host cell. The proposed mechanism [Figure 9] homologous to the Gram-negative TTSS, for Gram-positive pathogens, has an initial step that allows the bacteria to operate through the known secretion systems that involves the Tat and Sec pathways across the inner membrane. From here injectosomes are recruited to move these proteins from the cell membrane across the cell wall into the host. Once in the host cell wall environment, due to a higher presence of calcium, the collagenase seems to reveal a more rigid structure. This rearrangement of the enzyme structure allows for the secretion of the enzyme to occur at a more rapid rate through the channel, which seems to have a width of 65Å. (Green and Mecsas 2016)

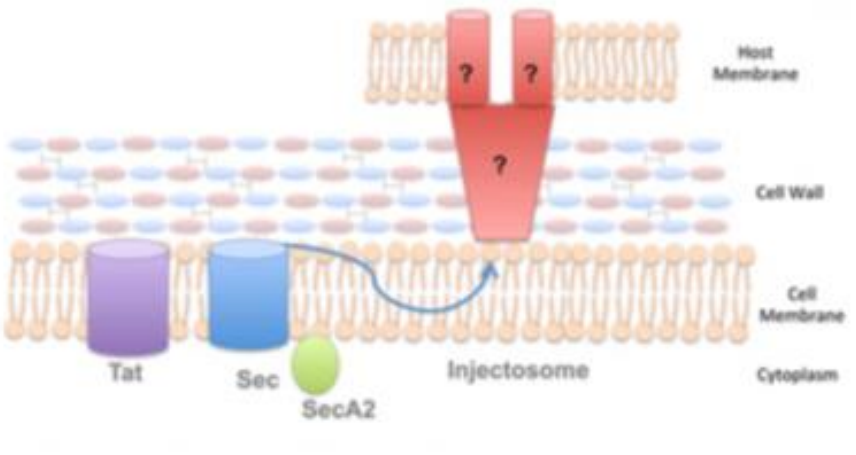

Figure 9: Secretion Systems in Gram-positive Bacteria Copyright permission granted for Figure 9 and 10 by the owner. Copyright © 2016 American Society for Microbiology. Used with permission. No further reproduction or distribution is permitted with the prior written permission of American Society for Microbiology.

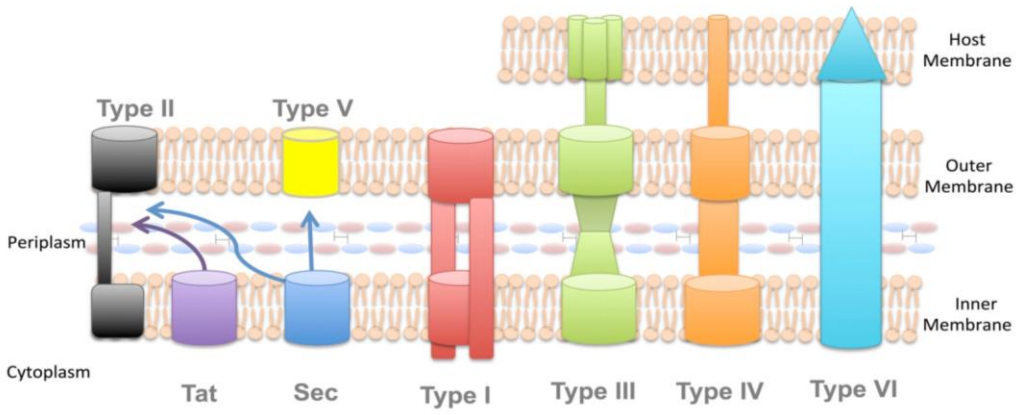

Figure 10: Type 2 Secretion System Proposed Mechanism. Copyright permission granted for Figure 9 and 10 by the owner. Copyright © 2016 American Society for Microbiology. Used with permission. No further reproduction or distribution is permitted with the prior written permission of American Society for Microbiology.

No other suggested systems for secretion have been confirmed. The only genome sequence data available for *Hathewaya* species is *Hathewaya proteolytica* which encodes type II, III and IV secretion systems. Thus, what was initially proposed to be a one-step system, could be a two-step approach which activates the protein to develop a more rigid structure within the high calcium periplasm region allowing for increased rate of delivery as the enzyme is injected from the periplasm across to the host ECM at record speed and initiating collagen binding in its active form.

This proposed system of delivery can be further supported with the use of additional instrumentation. SAXS instrumentation generates low resolution envelopes which allow for suggestive representation of the overall molecular shape. This, of course, can be very useful, but does not give exact amino acid residue positioning. SAXS results gave definite structure change throughout the various calcium environment. X-ray diffraction, on the other hand, can allow for a higher resolution result at its completion. High-resolution X-ray diffraction data can elucidate on residue level information. This technique places an x-ray beam on an atom of a molecule in

crystal form (Warren 1990). This process can be time consuming since the protein should be within an optimized environment for crystal growth. Aside from this there is also the phase problem, which occurs with the loss of information concerning the phase that can occur when measuring (Kleywegt 2000). When both techniques are utilized simultaneously a stronger argument can be made on the representation of the analyzed molecule. As conducted within this experimentation, SAXS generated envelopes allow for known X-ray crystal structures to be positioned appropriately within the envelope for further study of overall structure and often times function.

I. Collagenase G

The SAXS data were collected for the ColG at different pCa to mimic the calcium gradient that the protein experiences from the intra-bacterial to the extra-cellular fluid. As the pCa increases, the ColG begins to adopt a more elongated shape [Figures 11-14]. There is a significant difference in the domain linker distances as conditions change from pCa3 to pCa6 [Figures 11-14]. It is to be noted that the pCa 7 environment easily produced aggregation and thus is not ideal for analysis of this protein structure. The SAXS derived envelope for ColG at pCa3 [Figure 11] adopts a compact L shape. Superimposition of tandem-CBD derived envelope suggest that the base of L is where CBD2 (s3b) is located. PKD (s2) is positioned at the top of L. Domains are well-defined and little structural flexibility seems possible at this pCa. The overall shape of the pCa4 [Figure 12] envelope is very similar to that of pCa3. However, where pCa3 is very compact, pCa4 has a loose variation of the structure with an increase in the distance between the PKD(s2) domain and CBD1-CBD2 (s3as3b) domains. Slight variations were made for optimum envelope positioning with the known PDBs, which seem to offer less crowding

within the structure. Given the resolution of SAXS, the structural change between pCa3 to pCa4 is highly speculative. At pCa5 [Figure 13], the envelope continues to elongate, more so in the N-terminal region at the location of the s2 domain. The s3as3b domains stay close, but began to fan out, or lay down in a sense. At pCa6 [Figure 14], the envelope, which is not yet completely linear, gives a more elongated shape, with the domains in very specific individual regions of the envelope. The distance between the s3a and s3b are even more apparent in this calcium environment. PDB's 5IKU for CBD and 4TN9 for PKD were used to allow for optimum positioning of the envelopes for structural understanding.

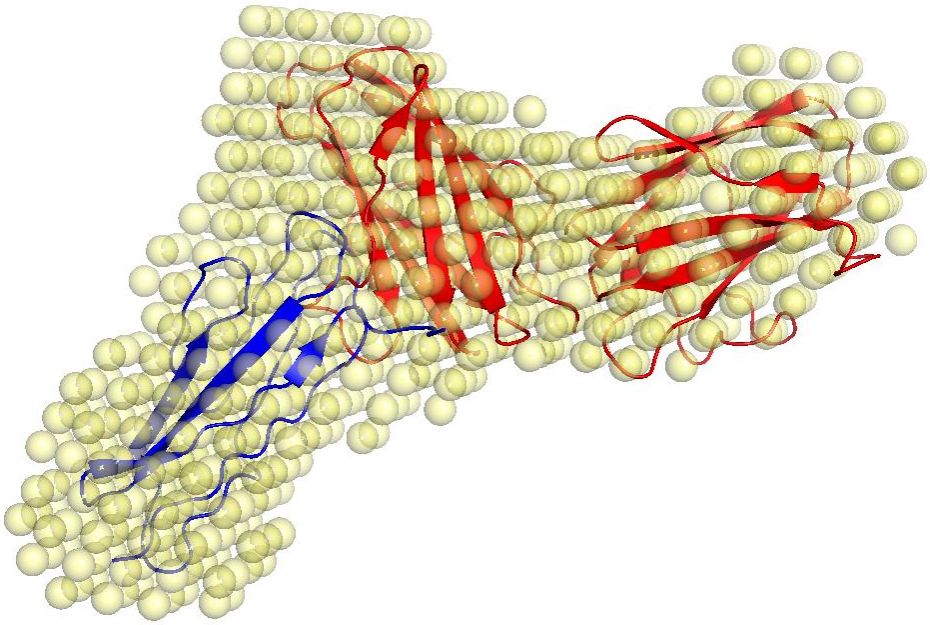

Figure 11: ColG pCa3 envelope positioned with s3as3b tandem CBD (red) and s2 PKD (blue).

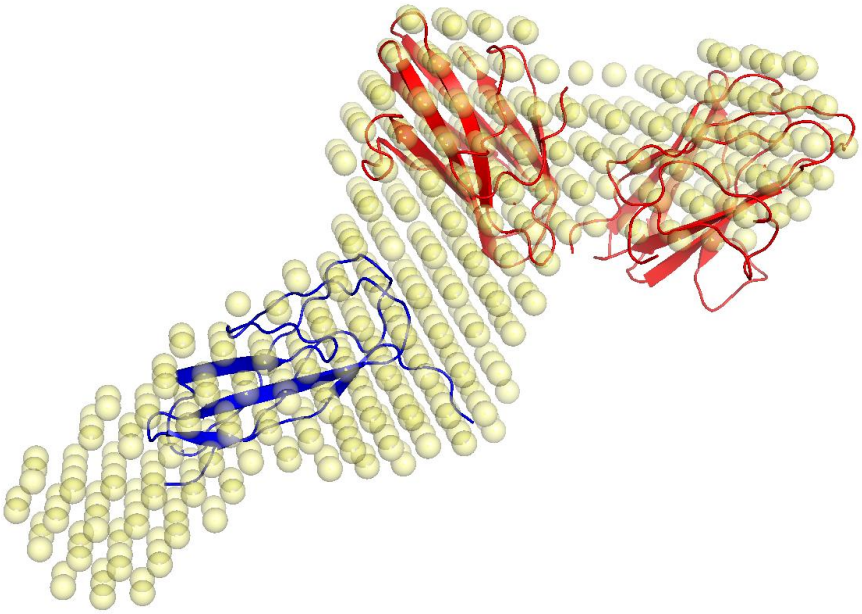

Figure 12: ColG pCa4 envelope positioned with s3as3b tandem CBD (red) and s2 PKD (blue).

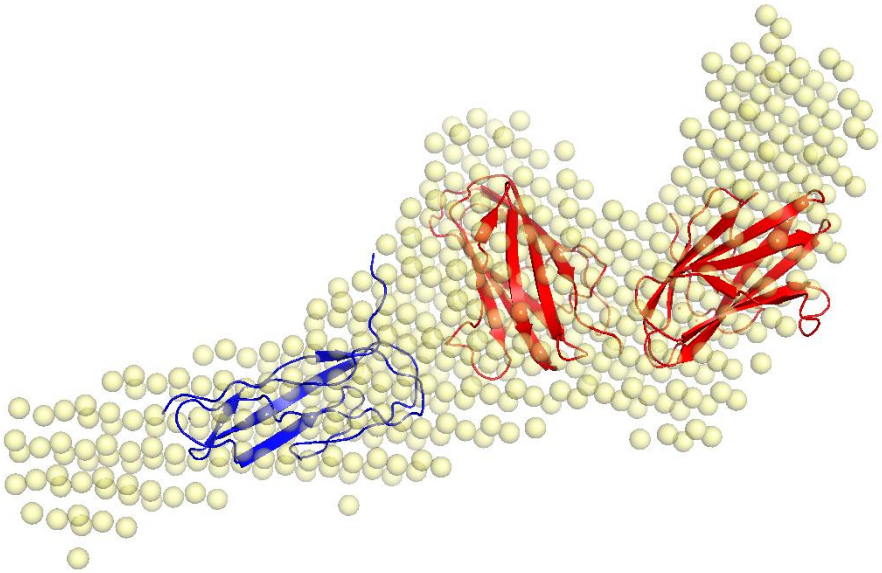

Figure 13: ColG pCa5 envelope positioned with s3as3b tandem CBD (red) and s2 PKD (blue).

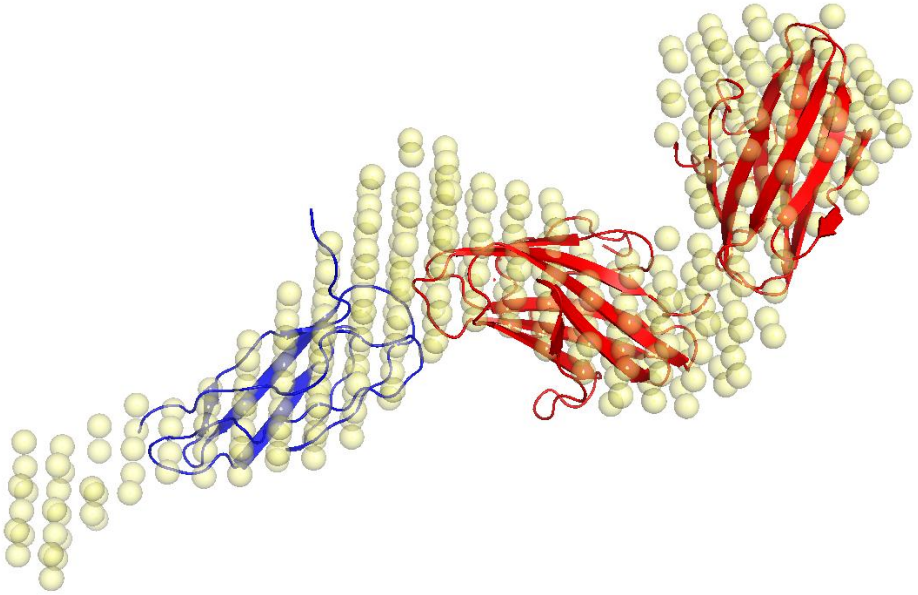

Figure 14: ColG pCa6 envelope positioned with s3as3b tandem CBD (red) and s2 PKD (blue).

II. Collagenase H

The structural change of the ColH at different pCa is not as discernible as that of ColG. However, there is still information to be obtained from these envelopes. Similar to ColG, as the ColH concentration of calcium decreases, or as the pCa increases, the collagenase envelope adopts a more elongated shape [Figures 15-19]. The noticeable differences in the inter-domain distances seem to be less apparent than with those of the ColG envelopes. However, as the pCa changes from 3-7 [Figure 15-19] we do notice an overall linear formation of the entire envelope. It can be seen at pCa 3 [Figure 15] the ColH molecule is not compact like that of the ColG at the same pCa, but it exhibits an L shape in the overall envelope. It is uncertain whether the base of the L is the location of the s3 CBD segment. Ohbayashi *et al.* published the SAXS of full-length ColG. A comparison suggests that s3 would likely be at the base of the L shaped envelope. At pCa 4, [Figure 16] not much variation is noticed in the overall shape. However, the PKD1 (s2a) and PKD2 (s2b) began to increase in distance and alignment from the CBD (s3). It can be further observed in pCa 5 [Figure 17] that the PKD1 and PKD2 segments began to position

themselves in a linear fashion almost perpendicular to the CBD. At pCa6 [Figure 18], PKD1 and PKD2 have now become completely linear and seems to begin to align themselves with the CBD. Finally, at pCa7 [Figure 19] of the ColH all segments can be seen aligned in linear fashion resembling a rod shape. This observation further supports the notion that in the presence of high calcium the ColH binding segments become rigid by what can be assumed to be the rearrangement of the linker. This adds to the theory that these enzymes are activated by the presence of calcium which is higher in host cells that then causes the segment linkers to rearrange into a more rigid orientation to allow the enzyme to actively bind and initiate collagenolysis. The PKD1-PKD2 segments alignment to CBD also leads me to assume the binding is primarily with in the function of the CBD. Within the varied pCa environments it can be seen that the eventual linear formation is produced by the conformity of the PKD segments to the CBD. PDB's 4U6T and 4U7K for PKD1 and 4JGU for PKD2, and 3JQW for CBD were used to allow for optimum positioning of the envelopes for structural understanding.

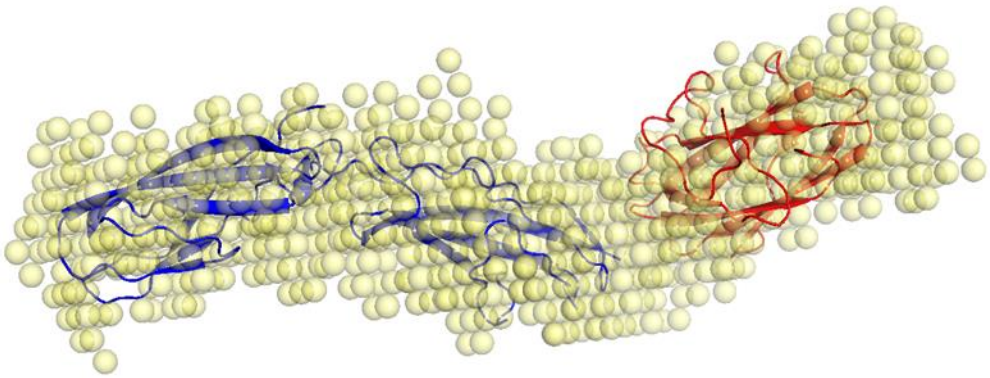

Figure 15: ColH pCa3 envelope positioned with s2as2b tandem PKD (blue) and s3 CBD (red).

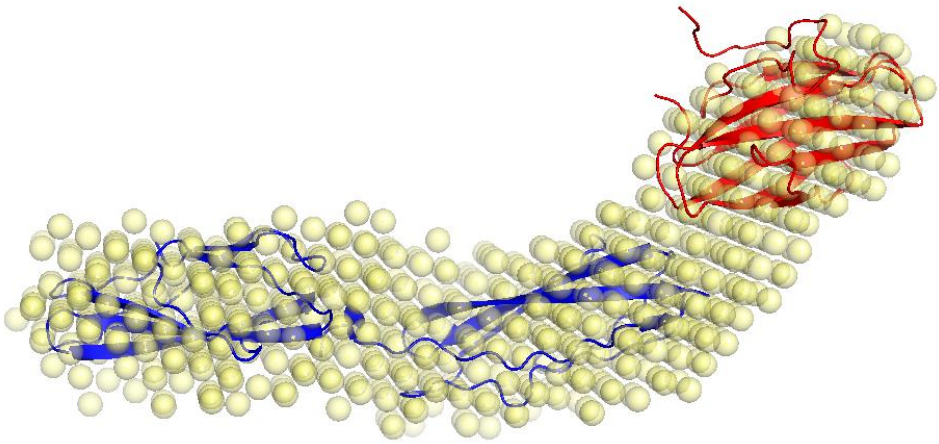

Figure 16: ColH pCa4 envelope positioned with s2as2b tandem PKD (blue) and s3 CBD (red).

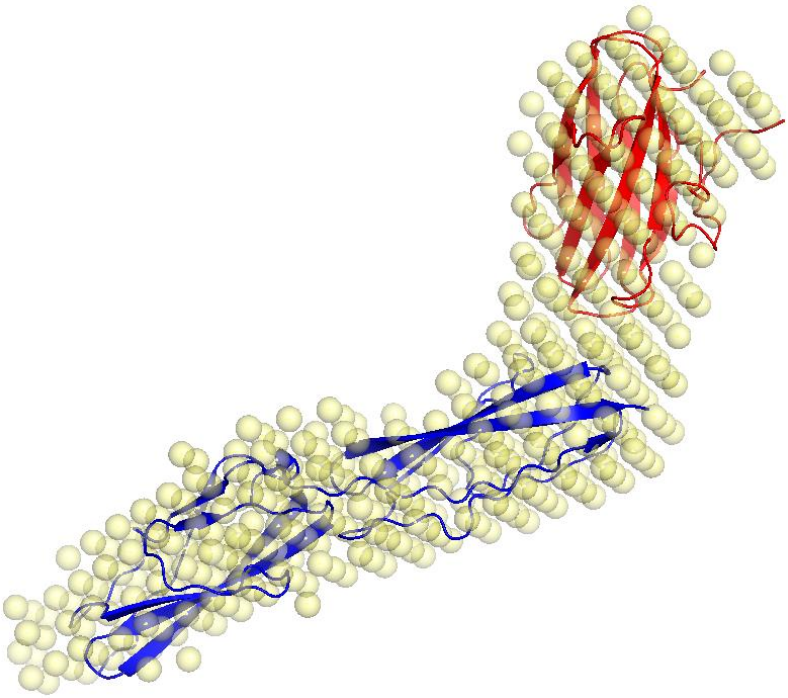

Figure 17: ColH pCa5 envelope positioned with s2as2b tandem PKD (blue) and s3 CBD (red).

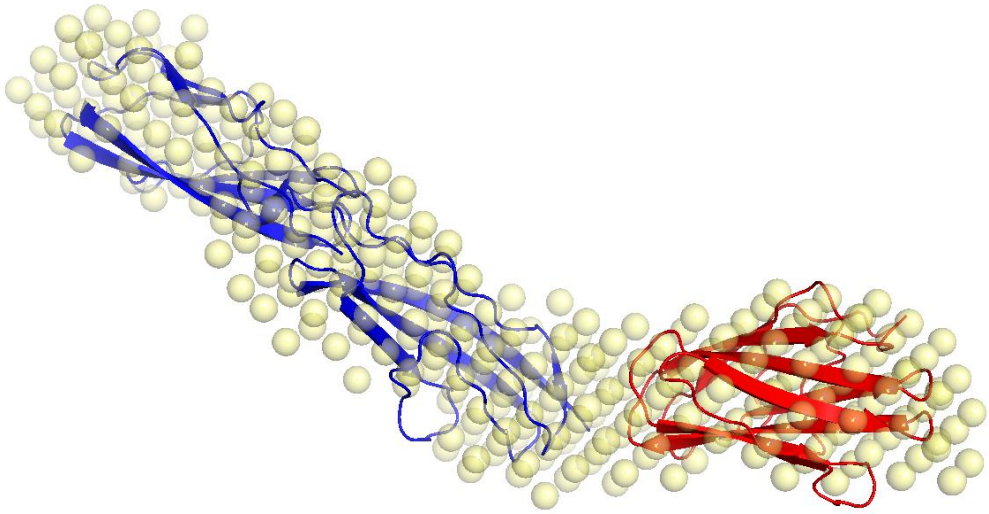

Figure 18: ColH pCa6 envelope positioned with s2as2b tandem PKD (blue) and s3 CBD (red).

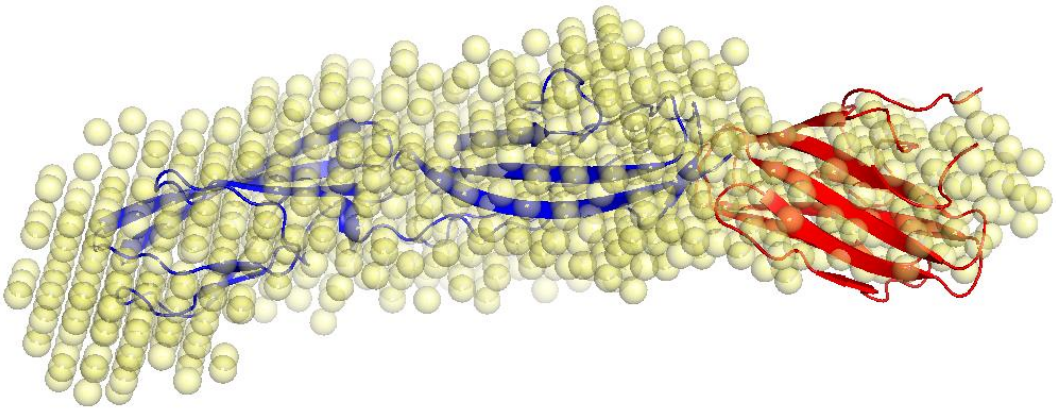

Figure 19: ColH pCa7 envelope positioned with s2as2b tandem PKD (blue) and s3 CBD (red).

H. histolytica genome is not available; however, a genome of *Hathewaya proteolytica* (*Clostridium proteolyticum*) was deposited in 2018. *H. proteolytica* encodes type II, III and IV secretion systems. The pore size of *Vibrio cholerae* Type II secretion system is 55 Å (Korotkov, Sandkvist et al. 2012). The pore size of Type III secretion system from *Pseudomonas aeruginosa* is 28-35 Å (Dacheux, Attree et al. 2001). The pore size of Type IV secretion system is 8 Å (Gomis-Ruth, Moncalian et al. 2002) (Fronzes, Christie et al. 2009) (Alvarez-Martinez and Christie 2009). The diameter of SAXS determined structure at high pCa is about 50 Å. Based on

the findings reported in this thesis, the opened pore size of secretion apparatus for *H. histolytica* should at least be 50 Å if collagenase adopts an elongated structure as seen. The catalytic module will also need to be elongated. The opened pore size of secretion apparatus needs to be as large as 120 Å to secrete fully activated collagenase; therefore, the full enzyme will also be likely to adopt an elongated structure. To secrete collagenases from cytosol of bacteria to ECM of host, bacteria may have adopted to take advantage of Ca^{2+} differential that exists across the bacterial membrane.

III. Binding Mechanism

Prior studies on the binding pattern of the ColG and ColH have suggested two modes of binding to collagen. The most recent studies (Caviness, Bauer et al. 2018) proposed ColG to bind two tropocollagen [Figure 20]. After superimposing the SAXS envelopes for PKD-CBD1-CBD2 at pCa3 with and without mini-collagen, three possible binding modes seem possible. The first position [Figure 20] is that of the recent studies from Caviness et al. This positioning seems to give a reasonable fit for PKD-CBD-CBD. The second position [Figure 21] places CBD1 and CBD2 (tandem; s3as3b) above the collagen-like molecule (POG). Also, PKD(s2) can be seen in front of or around the collagen-like molecule sitting beneath the tandem CBD molecules. The third position [Figure 22] places tandem CBD in the opposite orientation. The two CBD molecules are placed on or surrounding the collagen-like molecule in two individual positions. The PKD is now in a position above the tandem CBD and above the collagen-like molecule. The PKD does not have surface aromatic residues which leads one to believe that interaction with collagen may not be present. Although three possible orientations are present, it can be seen in figures 21 and 22 that the individual segments do not fully occupy the space of the envelope. The

envelopes for PKD-CBD1-CBD2 and PKD-CBD1-CBD2-mini-collagen superimposed the best, it seems, in figure 20 as published.

While superimposing the envelopes it was found that in the presence of calcium, the ColH binding segments (PKD1-PKD2-CBD) have not bound to collagen [Figure 23]. Although this was not within the scope of my research, SAXS envelope of PKD1-PKD2-CBD enabled the superimposition to be conducted, which lead to the final analysis that the PKD1-PKD2-CBD+mini collagen. The SAXS envelope does not seem to contain the mini collagen. When superimposed, the envelopes seem to be identical in size, shape, and length.

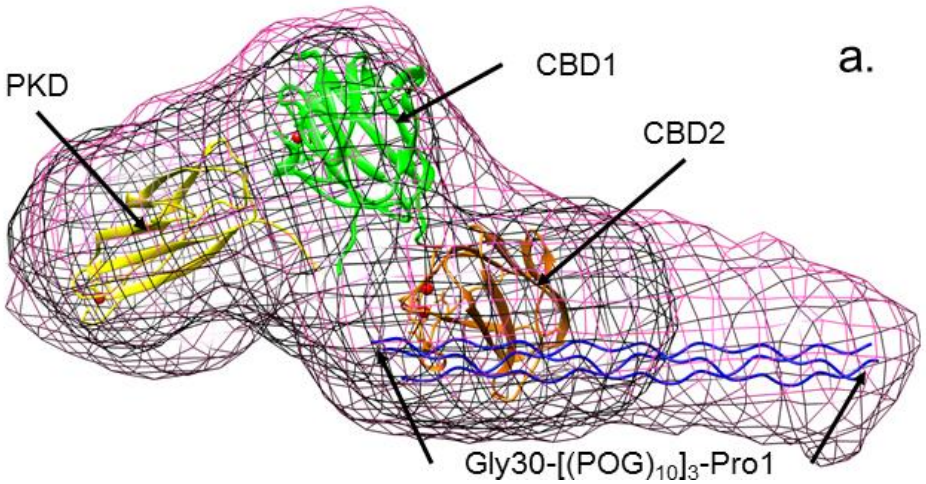

Figure 20: Recently proposed binding position for tandem CBD(s3as3b) and PKD1(s2). (Caviness, P. et al., 2018). Copyright permission granted for Figure 20 by the owner. Copyright © 2018, by John Wiley and Sons.

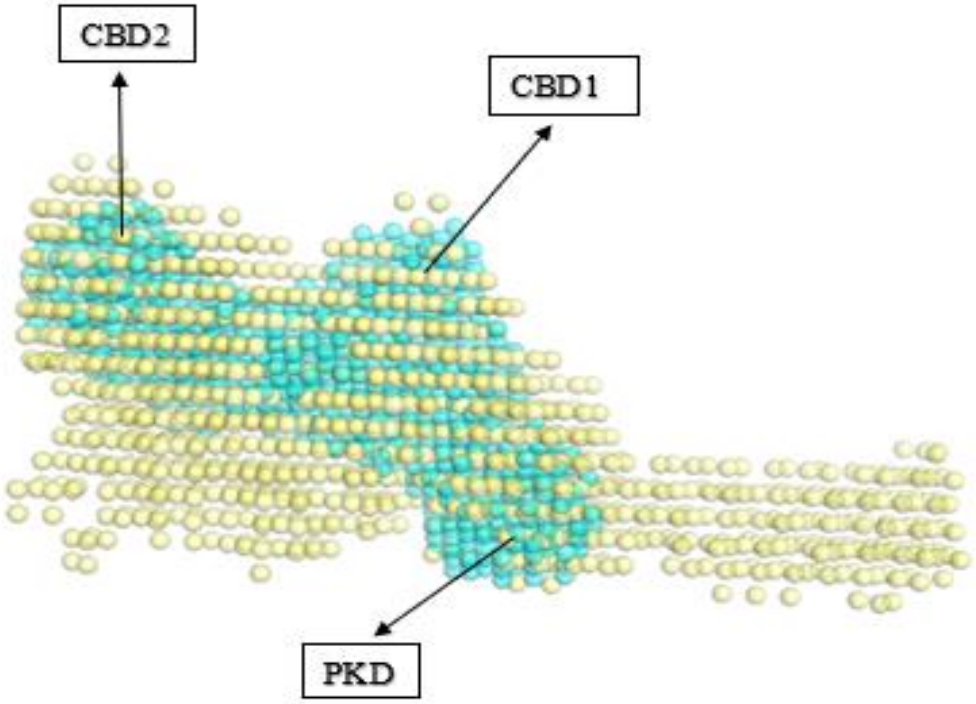

Figure 21: Binding position 1 for tandem CBD(s3as3b) and PKD1(s2).

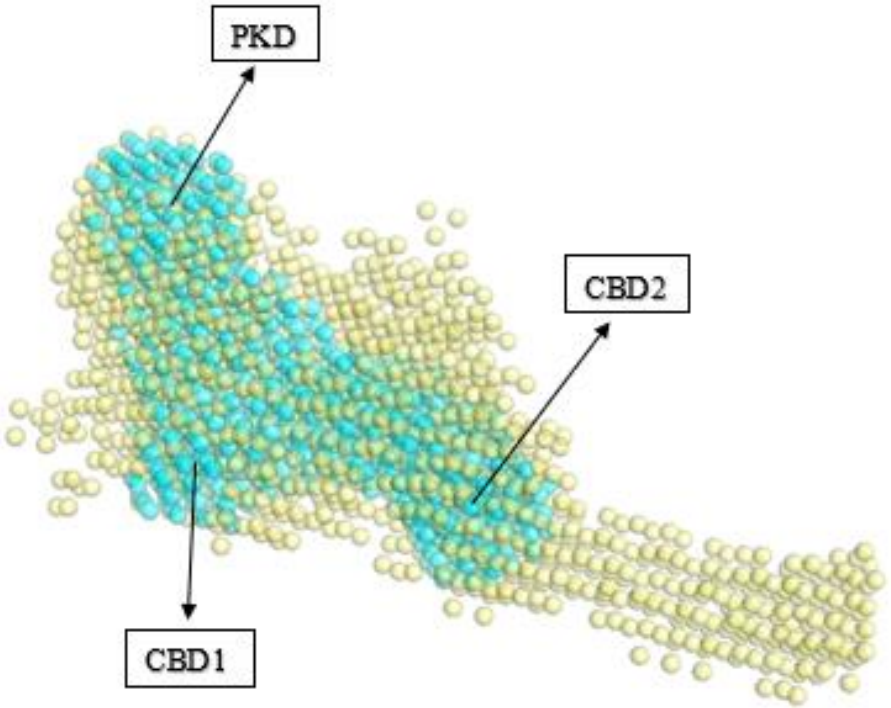

Figure 22: Binding position 2 for tandem CBD(s3as3b) and PKD1(s2).

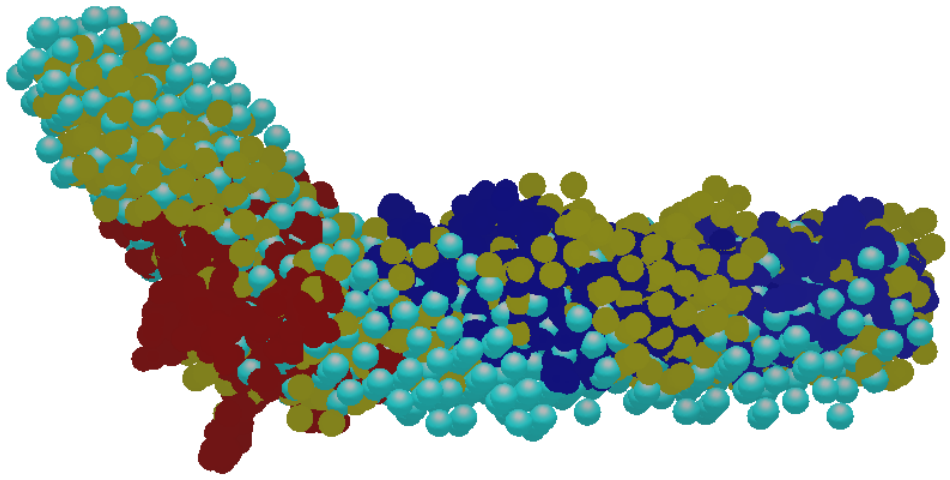

Figure 23: Superimposed envelops – Cyan: s2as2bs3, Yellow: s2as2bs3 with mini collagen, Blue: PKD1 and PKD2, Red: CBD.

Chapter 4: OTHER PROJECTS

I. Identifying Ruthenium Cross-linking Collagen Binding Sites

The collagen fiber has proven the most complex of the collagen forms to analyze appropriately. Due to its triple helical structure confirmation, any interaction studies with CBD become difficult to accomplish. The collagenase G binding domain, s3b, has been studied to determine the specific site of binding to collagen. It is known that these binding domains seek damaged areas of collagen to perform collagenlysis. However, a novel technique has been presented using a tris(bipyridine)ruthenium(II) as a photo-initiated protein cross-linking reaction to produce a tyrosine arene coupling or heteroatom-arene linkage (Geren, Hahm et al. 1991). Ruthenium is a potent one-electron oxidant and would be expected to oxidize residues such as tyrosine (Fancy and Kodadek 1999). The radical can then be attacked by cysteine or lysine groups to produce a heteroatom-arene linkage. Binding of s3b to an analogous ruthenium complex using this cross-linking approach may produce a method for analyzing site specific collagen binding. This ruthenium compound will not only initiate the binding of the CBD to collagen through this cross-linking reaction, but also produces a fluorescence gel band that will indicate the binding success with s3b as an initial step. In mass spectrometry (MS), confirmation of the exact binding site of the CBD to collagen will be determined following proteolysis. This study will produce much valuable information regarding the specific binding site of collagen to CBD regions. This will be the first proposed method of binding Ru, in solution, to the collagenase protein and using the complex for photo-initiated cross-linking. This will provide residue level identification, which could lead to significantly stronger collagen binding studies as well as further increased focus on clinical enhancement approaches for anchoring segments.

The s3b collagen binding domain (CBD) that is naturally in dimer form was reduced using tetramethylethylenediamine (TEMED). Once reduced, ruthenium was bound to the s3b CBD and confirmed. The newly bound CBD-ruthenium complex was then crosslinked with collagen. At each stage of binding, mass spectrometry was used to confirm its success.

Although binding was confirmed, the strength of binding was in question within this study. It is proposed, based on the results accumulated, that the binding has occurred, but maybe not all of the complex has bound or the binding has unbound itself. This would explain the decreased strength of the signal for the Ru-CBD bound complex that we have seen. Moving forward, an increased production of the Ru-CBD bound complex would need to be prepared before complete analysis can be done via mass spectrometry. Due to the weakness of the complex signal, if more of the complex is present our answer on this particular binding site can be far more definitive.

II. Crystallization of T. fusca Xyloglucanse for Structure Studies

Xyloglucans are a major hemicellulose component that is important to the structural integrity of the cell wall. Xyloglucans are classified as a XXXG-type or XXGG-type. The (XXXG)n classified types have three consecutive backbone residues that are substituted with xylose and a fourth unbranched backbone residue. Alternatively, the (XXGG)n type xyloglucans have two consecutive branched backbone residues and two unbranched backbone residues. The catalytic domain from Thermobifida fusca xyloglucan-specific endo-beta-1,4-glucanse is classified in glycosyl hydrolase family 74 (XEG74). XEG74 cleaves the glycosidic bond between G-X found in both (XXXG)n and (XXGG)n with inversion at the anomeric carbon. The function of this enzyme appears to be to break down the xyloglucan surrounding cellulose fibrils so that T. fusca can utilize the cellulose as a carbon source.

Orthohombic crystals belonging to space group I222 were previously obtained in PEG3350 solution. The structure was solved by molecular replacement using exo-beta-glycosidase (OXG-RCBH) as a search model. The structure, consisting of N-terminal and C-terminal domains, was refined to 2.0 Å resolution. Both domains adopt of seven-bladed beta-propeller fold suggesting a possible gene duplication event of the past. The active site is found in between the domains, and active site residues are provided from both domains. The residues involved in the inverting mechanism as well as substrate recognition are discussed. The procedure is currently being replicated for confirmation of optimum crystal conditions. Micro sized crystals have been obtained and have now moved into the refinement phase of the crystal formation. Once successful, macro sized 3D crystals will be diffracted from the in-house x-ray for definitive crystal structure analysis.

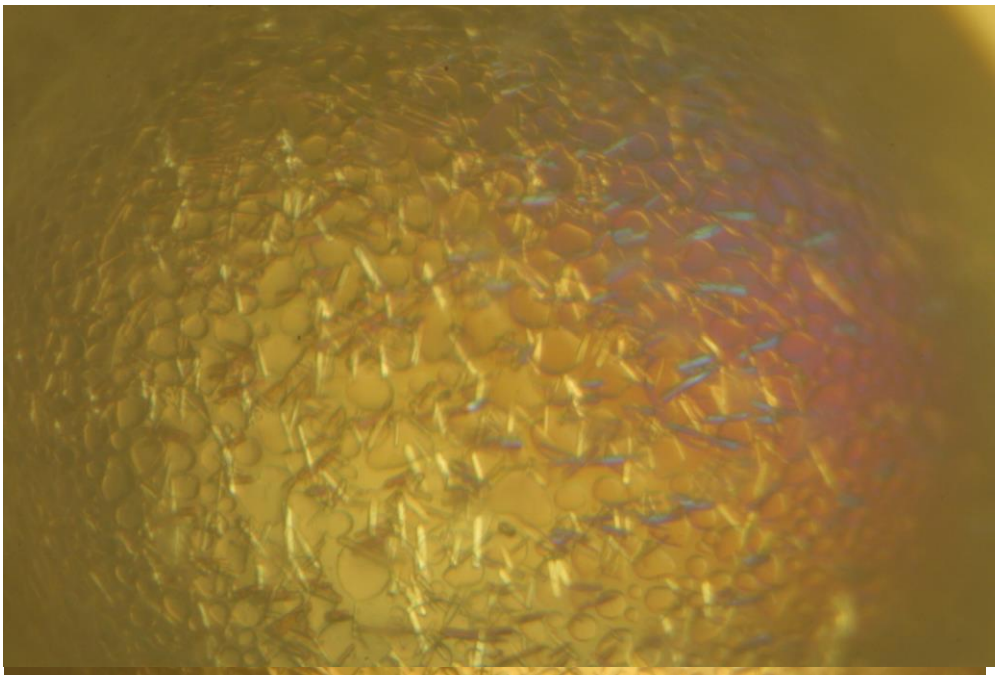

Figure 24: Refinement tray 10, well C3: 37% PEG3000 and 0.25M Sodium Sulfate

Chapter 5: REFERENCES

Addi, C., et al. (2016). "Design and Use of Chimeric Proteins Containing a Collagen-Binding Domain for Wound Healing and Bone Regeneration." Tissue Engineering: Part B **23**.

Alvarez-Martinez, C. E. and P. J. Christie (2009). "Biological Diversity of Prokaryotic Type IV Secretion Systems." Microbiology and Molecular Biology Reviews **73**(4).

Bauer, R., K. Janowska, K. Tamaka, O. Matsushita and J. Sakon (2017). "Activation and binding mechanisms of the tandem collagen-binding domain of ColG collagenase." The FASEB Journal **31**.

Bauer, R., K. Janowska, K. Taylor, B. Jordan, S. Gann, T. Janowski, E. Latimer, O. Matsushita and J. Sakon (2015). "Sturctures of Three Polycystic Kidney Disease-like Domains from Cl*ostridium* h*istolyticum* collagenases ColG and ColH." Acta Cryst **D71**: 565–577.

Bauer, R., J. J. Wilson, S. T. L. Philominathan, D. Davis, O. Matsushita and J. Sakon (2013). "Structural comparison of ColH and ColG collagen-binding domains from Clostridium histolyticum." Journal of Bacteriology **195**: 318-327.

Brown, E. M., P. M. Vassilev and S. C. Herbert (1995). "Calcium Ions as Extracellular Messengers." Cell **83**: 679-682.

Caviness, P., R. Bauer, K. Tanaka, K. Janowska, J. R. Roeser, D. Weir, J. Sanders, C. Ruth, O. Matsushita and J. Sakon (2018). "Ca2+ induced orientation of tandem collagen binding domains from clostridial collagenase ColG permits two opposing functions of collagen formation and retardation." The FEBS Journal **285**(17): 3254-3269.

Classen, S., G. L. Hura, J. M. Holton, R. P. Rambo, I. Rodic, P. J. McGuire, K. Dyer, M. Hammel, G. Meigs, K. A. Frankel and J. A. Tainer (2013). "Implementation and performance of SIBYLS: a dual endstation small-angle X-ray scattering and macromolecular crystallography beamline at the Advanced Light Source." J Appl Crystallogr **46**(Pt 1): 1-13.

Classen, S., G. L. Hura, J. M. Holton, R. P. Rambo, I. Rodic, P. J. McGuire, K. Dyer, M. Hammel, G. Meigs, K. A. Frankel and J. A. Tainer (2013). "Implementation and performance of SIBYLS: a dual endstation small-angle X-ray scattering and macromolecular crystallography beamline at the Advanced Light Source." Journal of Applied Crystallography **46**(Pt 1): 1-13.

Dacheux, D., I. Attree and B. Toussaint (2001). "Expression of ExsA in *trans* Confers Type III Secretion System-Dependent Cytotoxicity on Noncyctotoxic *Pseudomonas aeruginosa* Cystic Fibrosis Isolates." Infection and Immunity **69**(1).

Dyer, K. N., M. Hammel, R. P. Rambo, S. E. Tsutakawa, I. Rodic, S. Classen, J. A. Tainer and G. L. Hura (2014). "High-throughput SAXS for the characterization of biomolecules in solution: a practical approach." Methods Mol Biol **1091**: 245-258.

Eckhard, U. and H. Brandstetter (2011). "Polycystic Kidney Disease-like Domains of Clostridial Collagenases and Their Role in Collagen Recruitment." Biological Chemistry **392**(11): 1039-1045.

Eckhard, U., E. Schonauer and H. Brandstetter (2013). "Structural Basis for Activity Regulation and Substrate Preference of Clostridial Collagenases G, H, and T." The Journal of Biological Chemistry **288**(28): 20184-20194.

Eckhard, U., E. Schonauer, D. Nuss and H. Brandstetter (2011). "Structure of collagenase G reveals a chew-and-digest mechanism of bacterial collagenolysis." Nature Structural & Molecular Biology **18**(10): 1109-1114.

Fancy, D. A. and T. Kodadek (1999). "Chemistry for the analysis of protein-protein interactions: rapid and efficient cross-linking triggered by long wavelength light." Proceedings Of The National Academy Of Sciences Of The United States Of America **96**(11): 6020-6024.

Fronzes, R., P. J. Christie and G. Waksman (2009). "The Structural Biology of Type IV Secretion Systems." Nature Reviews Microbiology **7**: 703-714.

Fujimaki, H., K. Uchida, G. Inoue, M. Miyagi, N. Nemoto, T. Saku, Y. Isobe, K. Inage, O. Matsushita, S. Yagishita, J. Sato, S. Takano, Y. Sakuma, S. Ohtori, K. Takahashi and M. Takaso (2017). "Oriented collagen tubes combined with basic fibroblast growth factor promote peripheral nerve regeneration in a 15mm sciatic nerve defect rat model." Journal of Biomedical Materials Research Part A **105**(1).

Geren, L., S. Hahm, B. Durham and F. Millett (1991). "Photoinduced electron transfer between cytochrome c peroxidase and yeast cytochrome c labeled at Cys 102 with (4-bromomethyl-4'-methylbipyridine)[bis(bipyridine)]ruthenium2+." Biochemistry **30**(39): 9450-9457.

Gomis-Ruth, F. X., G. Moncalian, F. de la Cruz and M. Coll (2002). "Conjugative Plasmid Protein TrwB, an Integral Membrane Type IV Secretion System Coupling Protein detailed structural features and mapping of the active site cleft." The Journal of Biological Chemistry **277**(9): 7556-7566.

Green, E. R. and J. Mecsas (2016). "Bacterial Secretion Systems – An Overview. M*icrobiology Spectrum*." Microbiol Spectr **1**.

Holland, I. B., H. E. Jones, A. K. Campbell and A. Jacq (1999). "An Assessment of the Role of Intracellular Free Ca2+ in E. coli." Biochimie **Volume 81**(Issues 8–9): 901-907.

Kleywegt, G. J. (2000). "Validation of Protein Crystal Structures." Acta Cryst **D56**: 249-265.

Konarev, P., M. Petoukhov, V. Volkov and D. Svergun (2006). "ATSAS 2.1, A Program Package for Small-Angle Scattering Data Analysis." Journal of Applied Crystallography **39**: 277-286.

Korotkov, K., M. Sandkvist and W. G. J. Hol (2012). "The Type II Secretion System: Biogenesis, Molecular Architecure and Mechanism." Nature Reviews Microbiology **10**: 336-351.

Lawson, P. A. and F. A. Rainey (2016). "Proposal to restrict the genus Clostridium Prazmowski to Clostridium Butyricum and related species." International Journal of Systematic and Evolutionary Microbiology **66**: 1009–1016.

Matsushita, O., C.-M. Jung, J. Minami, S. Katayama, N. Nishi and A. Okabe (1998). "A study of the collagen-binding domain of a 116-kDa Cl*ostridium histolyticum c*ollagenase." The Journal of Biological Chemistry **273**: 3643-3648.

Matsushita, O., T. Koide, R. Kobayashi, K. Nagata and A. Okabe (2001). "Substrate Recognition by the Collagen-binding Domain of Clostridium histolyticum Class 1 Collagenase." The Journal of Biological Chemistry **276**(12): 8761-8770.

Maurer, P. and E. Hohenester (1997). "Structural and Functional Aspects of Calcium Binding in Extracellular Matrix Proteins." Matrix Biology **Volume 15**(Issues 8–9): 569-580.

Melville, S. (2015). Characterization of a Type II Secretion System in a Gram-Positive Pathogen. Virginia Polytechnic Institute and State University (Blacksburg, VA), National Institute of Health.

Nicholson, C. (1980). "Modulation of Extracellular Calcium and Its Functional Implications." Federation Proceedings **39**(5): 1519-1523.

Nishi, N., O. Matsushita, K. Yuube, H. Miyanaka, A. Okabe and F. Wada (1998). "Collagen-binding growth factors: Production and characterization of functional fusion proteins having a collagen-binding domain." PNAS **95**(12): 7018-7023.

Ohbayashi, N., T. Matsumoto, H. Shima, G. M., K. Watanabe, A. Yamato, Y. Katona, K. Igarashi, Y. Yamagata and K. Murayama (2013). "Solution structure of Clostridial Collagenase H and Its Calcium-Dependent Global Conformation Change." Biophys **104**: 1538-1545.

Ohbayashi, N., N. Yamagata, M. Goto, K. Watanabe, Y. Yamagata and K. Murayamab (2012). "Enhancement of the Structural Stability of Full-Length Clostridial Collagenase by Calcium Ions." Applied and Environmental Microbiology **78**(16): 5839-5844.

Otwinowski, Z. and W. Minor (1997). "Processing of X-ray Diffraction Data Collected in Oscillation Mode." Methods of Enzymology **276**: 307-326.

Philominathan, S., T. L., T. Koide, K. Hamada, H. Yasui, S. Seifert, O. Matsushita and J. Sakon (2009). "Unidirectional binding of clostridial collagenase to triple helical substrates." Journal of Biological Chemistry **284**(16): 10868-10876.

Philominathan, S. e. a. (2012). "Bacterial Collagen-Binding Domain Targets Undertwisted Regions of
Collagen." Protein Science **21**: 1554-1565.

Ponnapakkam, T. e. a. (2014). "Parathyroid hormone linked to a collagen binding domain (PTH-CBD) promotes hair growth in a mouse model of chemotherapy-induced alopecia in a dose-dependent manner." Anticancer Drugs **25**(7): 819-825.

Ruth, C. E. and J. Sakon (2017). "Multi-Domain Dynamic Studies of Calcium Bound Polycystic Kidney Disease-Like and Collagen Binding Domains." The FASEB Journal **31(1_supplement)**: 1695.

Sekiguchi, H. e. a. (2018). "Basic Fibroblast Growth Factor Fused with Tandem Collagen-Binding Domains from Cl*ostridium histolyticum Co*llagenase ColG Increases Bone Formation." *BioMed Research International*.

Sides, C. (2012). "Probing the 3-D Structure, Dynamics, and Stability of Bacterial Collagenase Collagen Binding Domain (apo- versus holo-) by Limited Proteolysis MALDI-TOF MS." J Am Soc Mass Specrom **23**(3): 505-519.

Spiriti and v. D. Vaart (2010). "Mechanism of the Calcium-Induced trans-cis Isomerization of a Non-Prolyl Peptide Bond in Clostridium histolyticum Collagenase." Biochemistry **49**: 5314-5320.

Tsuruta, H. and J. E. Johnson (2006). International Tables for Crystallography Volume F: Crystallography of biological macromolecules.

Uchida, K. e. a. (2013). "Acceleration of bone formation during bone fracture healing by injectable collagen powder and human basic fibroblast growth factor containing a collagen-binding domain from *Clostridium histolyticum* collagenase." *Journal of Biomedical Materials Research* **102**(9).

Uchida, K. e. a. (2015). "Acceleration of callus formation during fracture healing using basic fibroblast growth factor-kidney disease domain collagen-binding domain fusion protein combined with allogenic demineralized bone powder." *Journal of Orthopaedic Surgery and Research*.

Uchida, K. e. a. (2016). "Acceleration of bone formation during fracture healing by poly(pro-hyp-gly)10 a nd basic fibroblast growth factor containing polycystic kidney disease and collagen-binding domains from Cl*ostridium histolyticum co*llagenase." *Journal of Biomedical Materials Research Part A* **104**(6).

Wang, Y. e. a. (2010). "Mechanistic Insight into the Function of the C-terminal PKD Domain of the Collagenolytic Serine Protease Deseasin MCP-01 f rom Deep Sea Ps*eudoalteromonas sp. SM*9913. Binding of the PKD Domain to Collagen Results in Collagen Swelling but Does Not Unwind the Collagen Triple Helix." The Journal of Biological Chemistry **285**: 14285-14291.

Warren, B. E. (1990). Diffraction, Courier Corporation.

Wilson, J. J., O. Matsushita, A. Okabe and J. Sakon (2003). "A Bacterial Collagen-Binding Domain with Novel Calcium-Binding Motif Controls Domain Orientation." *The EMBO Journal* **22**(8): 1743-1752.

Yan, Z., M. Yin, D. Xu, Y. Zhu and X. Li (2017). "Structural insights into the secretin translocation channel
in the type II secretion system." Nature Structural & Molecular Biology **24**(2): 177-183.